LARGE KUIPER BELT OBJECTS: THE MAUNA KEA 8K CCD SURVEY

DAVID JEWITT
Institute for Astronomy, 2680 Woodlawn Drive, Honolulu, HI 96822; jewitt@ifa.hawaii.edu

JANE LUU
Department of Astronomy, Harvard University, 60 Garden Street, Cambridge, MA 02138; luu@cfa.harvard.edu

AND

CHADWICK TRUJILLO
Institute for Astronomy, 2680 Woodlawn Drive, Honolulu, HI 96822; chad@ifa.hawaii.edu
Received 1997 November 18; revised 1998 January 20

ABSTRACT

We describe a large-area ecliptic survey designed to assess the sky-plane surface density of bright Kuiper Belt objects. We used an 8192×8192 pixel CCD mosaic to image 51.5 deg^2 to a 50% detection threshold red magnitude $m_R = 22.5$. Thirteen new Kuiper Belt objects were identified in the survey, including some of the brightest and, presumably, largest known examples. We use Monte Carlo models to assess the effects of observational bias in our survey and to examine (1) the size distribution of bright objects in the Kuiper Belt, (2) the possible existence of a cutoff in the size distribution at large radii, (3) the intrinsic ratio of Plutinos to nonresonant ("classical") Kuiper Belt objects, (4) the intrinsic ratio of populations in the 3:2 and 2:1 mean motion resonances, and (5) the radial extent of the Kuiper Belt.

Key words: celestial mechanics, stellar dynamics — Kuiper belt objects — minor planets, asteroids

1. INTRODUCTION

Recent ground-based observations have unveiled a large number of bodies in orbit beyond Neptune (Jewitt & Luu 1993, 1995; Irwin, Tremaine, & Żytkow 1995; Williams et al. 1995; Jewitt, Luu, & Chen 1996), in a region now widely known as the Kuiper Belt. Population estimates based on limited sampling of the ecliptic suggest that more than 70,000 bodies with diameters ≥ 100 km are to be found in the 30–50 AU distance range, with a combined mass of order 0.1 Earth masses (Jewitt et al. 1996). While uncertain, this estimate shows unambiguously that the trans-Neptunian solar system is a richly populated region deserving of intensive observational study. Ground-based observations have already revealed dynamical substructure in the Kuiper Belt. Evidence exists for three separate dynamical classes of trans-Neptunian object:

1. Residents of the "classical" Kuiper Belt lie beyond about 40 AU and occupy low-inclination orbits of modest eccentricity. These objects remain far from Neptune and appear to be dynamically stable over the lifetime of the solar system (Holman & Wisdom 1993; Duncan, Levison, & Budd 1995; Morbidelli, Thomas, & Moons 1995).

2. In contrast, objects in mean motion resonances approach (and even cross) the orbit of Neptune but are protected from close encounters with the planet, as is Pluto (Malhotra 1995). These resonance objects constitute a distinct dynamical class. Approximately 35% (i.e., 25,000) of the known Kuiper Belt objects (KBOs) reside in the 3:2 resonance (the so-called Plutinos; Jewitt & Luu 1995; Jewitt et al. 1996). The discovery of the Plutinos has provoked a number of theories about the origin and long-term evolution of resonant structure in the outer solar system (Malhotra 1995, 1996; Levison & Stern 1995) and has revealed the true nature of Pluto as the largest known member of the Plutino family.

3. Most recently (and as part of the present wide-field survey), we have identified a third distinct dynamical class in 1996 TL$_{66}$ (Luu et al. 1997). Members of this class of

"SKBOs" (scattered Kuiper Belt objects) follow large, highly eccentric, and inclined orbits generally with perihelion distances greater than 30 AU. They may constitute a chaotic swarm of bodies scattered outward by Neptune in the early phases of the solar system (Torbett 1989; Ip & Fernandez 1991; Duncan & Levison 1997). The number of SKBOs is highly uncertain, but a population of order 6×10^3 (500 km diameter or larger) is suggested by the discovery of 1996 TL$_{66}$ (Luu et al. 1997). In absolute numbers, the SKBOs may dominate the trans-Neptunian region. However, the SKBOs appear rare in magnitude-limited surveys because their large, eccentric orbits render them invisible except when near perihelion.

Much work remains to be done to establish the precise nature, origin, and significance of dynamical substructure in the Kuiper Belt. One problem in the study of the global properties of the trans-Neptunian solar system is that only a fraction of the known KBOs were identified in controlled surveys of known depth and areal coverage (specifically, seven objects from Jewitt & Luu 1995, two from Irwin et al. 1995, and 15 from Jewitt et al. 1996). We have embarked on a large survey with five main scientific goals: (1) to determine the luminosity function and size distribution of bright KBOs, (2) to search for evidence of an upper size cutoff that might indicate premature termination of the growth phase, (3) to assess the intrinsic (as opposed to apparent) ratio of Plutinos to classical KBOs, (4) to measure the intrinsic ratio of the populations of the 2:1 and 3:2 mean motion resonances, and (5) to examine the radial extent of the Kuiper Belt. As a side benefit, this survey will secure a sample of KBOs bright enough for relatively easy physical study using large ground-based telescopes.

2. OBSERVATIONS

Bright KBOs are comparatively rare. To find them, we must survey areas of sky much larger than feasible using conventional 2048×2048 pixel format CCDs. Accordingly, the present work is based on a new UH 8192×8192 pixel

(hereafter 8K) CCD array built at the Institute for Astronomy (Luppino et al. 1996). This device consists of eight 2048 × 4096 pixel Loral chips, with 15 μm square pixels, and with a gap between chips of about 1 mm. These are thick chips, with a resulting high cosmic-ray detection rate (about four per chip per second) and a peak quantum efficiency of ≈ 0.4. In addition, the chips are cosmetically inferior to the smaller Tektronix devices previously employed in this work. However, these disadvantages are outweighed for survey work by the sheer size of the 8K array.

Observations were taken at the University of Hawaii (UH) 2.2 m telescope atop Mauna Kea. We placed the 8K array at the f/10 Cassegrain focus. The system throughput at this position is very high, with light losses only from two optical elements (the dewar window and a filter) in addition to the two reflections from telescope mirrors. To further enhance the throughput, a custom broadband "VR" filter with high transmission in the 5000–7000 Å wavelength range was used for all observations (see Jewitt et al. 1996). The CCD was binned in 3 × 3 mode (reducing the readout time to about 1 minute) to obtain an image scale of $0\!\!''\!405 \pm 0\!\!''\!002$ per binned pixel. Typical seeing was $0\!\!''\!8$–$1\!\!''\!0$ FWHM, so that Nyquist sampling of the point-spread function was obtained. A field of view of $18\!\!'\!4 \times 18\!\!'\!4$ (0.094 deg^2) was obtained.

Flat fields were constructed from the median of a set of spatially offset images of the evening twilight sky. Photometric calibration was obtained from measurements of standard stars from Landolt (1992). The eight CCDs have different photometric and cosmetic properties, and so each was calibrated separately. We found that the photometric zero points of the CCDs differed by as much as 0.5 mag but that the differences were stable from night to night and month to month. The only photometric instabilities of note were occasional flat-field defects caused by windblown volcanic dust settling on the VR filter during the observations.

Survey images were taken in the ecliptic and near opposition, over a total sky area of 51.5 deg^2. This observing geometry is optimal since, at opposition, the angular rate of retrograde motion provides a direct measure of the heliocentric distance. A fixed integration time of 150 s was employed. To maximize observing efficiency, the survey integrations were taken without use of the autoguider. This resulted in a small but measurable ($0\!\!''\!1$–$0\!\!''\!2$) degradation in the image quality. Sequences of 10–15 consecutive images, each offset by 20' in declination, were repeated three times in order to search for slow-moving objects. After flat-fielding, the images were co-aligned and lists of all objects in each field were made by our Moving Object Detection Software (MODS; Trujillo & Jewitt 1998). The object lists were then culled to eliminate cosmic rays and noise clumps. Finally, we visually examined a MODS-generated list of candidate moving objects. In the present survey, MODS searched for linear, correlated motions at speeds 2" hr$^{-1} \leq d\theta/dt \leq 24$" hr^{-1}, corresponding approximately to heliocentric distances 5 AU $\leq R \leq$ 70 AU. Newly detected objects were scheduled for follow-up observations within the discovery observing run. Second-month and later observations were attempted from the UH 2.2 m, as well as from the 1.2 m telescope at Mount Hopkins, Arizona (mostly by C. W. Hergenrother and W. R. Brown). A special feature of the present survey over its predecessors is that many of the detected objects are bright enough to be observed with very modest telescopes. In this regard, we benefited greatly from observational efforts by W. Offutt using his 0.6 m telescope in New Mexico.

The detection efficiency of the survey was measured by searching for synthetic slow-moving objects added to real CCD images, as described by Trujillo & Jewitt (1998). The detection efficiency curve for Kuiper Belt objects is plotted in Figure 1. Two features are especially worthy of note. First, the maximum detection efficiency (≈ 0.9) is limited by objects that either move off the edge of the CCD or move onto one of the dead columns that afflict several of the CCDs with particular severity. Second, the decline in detection efficiency at larger magnitudes is spread over more than a full magnitude, with a detection efficiency equal to half the maximum value at $m_R = 22.5$. This gradual decline is primarily a result of averaging the different limiting sensitivities of the eight CCDs, which were combined to produce Figure 1.

Orbital elements of the 13 objects discovered with the 8K CCD are listed in Table 1. These elements are drawn from the Minor Planet Electronic Circulars by B. Marsden of the Harvard-Smithsonian Center for Astrophysics. It should be noted that the elements are subject to revision as new astrometric observations become available. In particular, the elements of objects observed only within a single opposition are liable to substantial correction. A plot of the semimajor axis versus eccentricity plane is given in Figure 2, with single- and multiopposition orbits distinguished. An alternative view, showing the KBOs projected onto the plane of the ecliptic, is given in Figure 3.

The image profiles of all 13 new KBOs were indistinguishable from those of adjacent field stars. Magnitudes of the new KBOs were determined using synthetic photometry apertures $1\!\!''\!6$ in radius, with the sky level determined in an annulus having inner and outer radii of $1\!\!''\!6$ and $8\!\!''\!0$, respectively. Images that appeared confused with background stars or galaxies were rejected. Magnitudes determined on different nights were found to be consistent within the
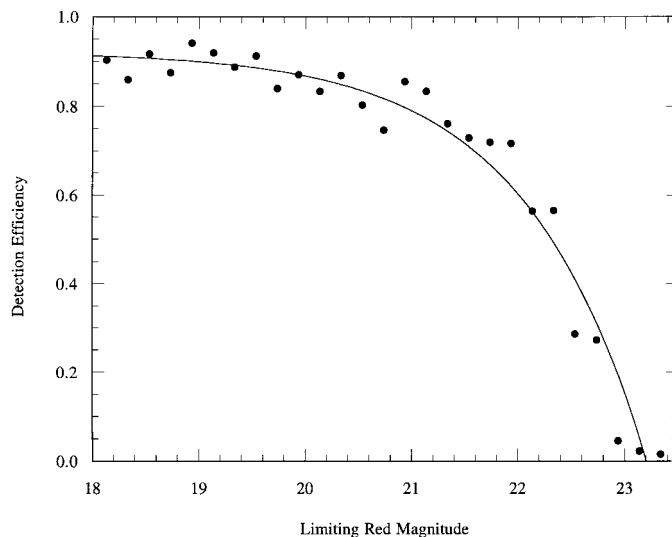

FIG. 1.—Detection efficiency with the 8K CCD array as a function of apparent red magnitude, m_R. The efficiency was determined by using the MODS software (Trujillo & Jewitt 1998) on a set of artificial KBOs (speeds 2" hr$^{-1} \leq d\theta/dt \leq 6$" hr^{-1}) added to real survey data. The integration time was 150 s through the VR 5000–7000 Å filter, with median seeing $0\!\!''\!8$ FWHM.

TABLE 1

ORBITAL PARAMETERS OF THE NEW OBJECTS

Object	q (AU)	Q (AU)	Epoch	M (deg)	ω (deg)	Node (deg)	i (deg)	e	a (AU)	Opp.[a]	Reference[b]	Discovery Date
1996 TL$_{66}$	35.03	134	1997 Dec 18	358.4	184.6	217.8	24.0	0.586	84.685	2	MPC 30690	1996 Oct 9
1996 TO$_{66}$	38.37	48.81	1997 Dec 18	108.6	244.2	355.2	27.3	0.120	43.590	2	MPC 30690	1996 Oct 12
1996 TP$_{66}$	26.38	53.05	1997 Dec 18	357.0	74.6	316.6	5.7	0.336	39.712	2	MPC 30690	1996 Oct 11
1996 TQ$_{66}$	34.59	44.71	1997 Dec 18	356.6	22.2	10.7	14.6	0.128	39.651	2	MPC 30690	1996 Oct 8
1996 TR$_{66}$	33.17	52.10	1997 Dec 18	326.7	73.3	342.9	12.3	0.222	42.636	2	MPC 30690	1996 Oct 8
1996 TS$_{66}$	38.23	50.09	1997 Dec 18	336.7	142.1	285.8	7.4	0.134	44.160	2	MPC 30690	1996 Oct 12
1997 CW$_{29}$	36.27	42.48	1997 Feb 21	179.65	188.5	110.7	19.0	0.079	39.375	(27)	MPC 30244	1997 Feb 8
1997 CV$_{29}$	39.98	48.46	1997 Feb 21	0.05	16.4	120.8	7.8	0.096	44.227	(60)	MPC 30244	1997 Feb 6
1997 CU$_{29}$	41.87	44.79	1997 Dec 18	180.0	303.6	349.9	1.5	0.034	43.331	2	E 1997-S12	1997 Feb 6
1997 CT$_{29}$	40.80	44.98	1997 Feb 1	187.37	238.2	68.7	1.0	0.049	42.894	(30)	MPC 30244	1997 Feb 2
1997 CS$_{29}$	43.45	43.96	1997 Dec 18	292.9	238.6	304.3	2.3	0.006	43.704	2	E 1997-S11	1997 Feb 3
1997 CR$_{29}$	41.99	41.99	1997 Feb 21	0.00	8.0	127.6	20.2	0.00	41.996	(63)	MPC 30244	1997 Feb 3
1997 CQ$_{29}$	41.15	47.67	1997 Feb 21	3.51	18.4	132.8	2.9	0.073	44.412	(57)	MPC 29883	1997 Feb 4

NOTE.—Orbital parameters from B. G. Marsden.

[a] Number of oppositions at which the object has been observed. If observations have been made at one opposition only, the arc length in days is given in parentheses.

[b] (MPC) Minor Planet Circular; (E) Minor Planet Electronic Circular.

photometric uncertainties. In Table 2, we present the mean of all magnitudes measured for each object, together with the standard deviation on the mean and an indication of the number of measurements. Optical colors of KBOs vary from nearly neutral ($V - R \approx 0.3$) to very red ($V - R \approx 0.7$), leading to an additional, systematic uncertainty in the R magnitude derived from the present broadband VR observations (Luu & Jewitt 1996). We estimate that this uncertainty amounts to 0.2 mag. In Table 2, the mean apparent red magnitude has also been converted to absolute magnitude, H, using the H-G relations of Bowell et al. (1989) with $G = 0.15$ (as appropriate for low-albedo objects). The maximum phase angle attained by KBOs at 30 AU is $1°.9$, so that the phase correction is small and the choice of G is not critical.

3. DISCUSSION

Surface densities of KBOs are summarized in Table 3. In

addition to the CCD detections of the modern era, there exist several photographic constraints at magnitudes $m_R \leq 20$ (Tombaugh 1961; Kowal 1989; see also Luu & Jewitt 1988). However, the photographic detection of faint, slow-moving objects is notoriously difficult and, most importantly, is not easily quantified. As a result, we are less confident of the significance of the photographic surveys than of the CCD work described above. For this reason, we base our physical interpretations only on the new (Table 3) and previously published (Table 4) CCD data. At the end of this section, we will show that the photographic constraints, with one exception, require no modification of the conclusions obtained from the CCD data alone. A *Hubble Space Telescope* observation by Cochran et al. (1995) has been reexamined and brought into serious question by Brown, Kulkarni, & Liggett (1997). In view of its uncertain signifi-
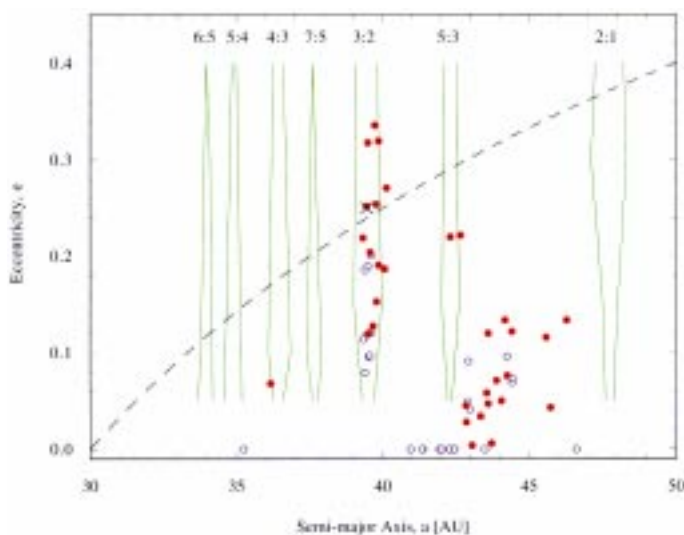

FIG. 2.—Semimajor axis vs. eccentricity for Kuiper Belt objects. Filled circles denote multiopposition orbits. Open circles denote orbits computed from astrometry taken within a single opposition. Pluto is marked by a cross. Neptune is at $(a, e) = (30\ \text{AU}, 0)$. The dashed line marks $q = 30$ AU. Objects above the line are Neptune crossers. Scattered Kuiper Belt object 1996 TL$_{66}$ is off scale [$(a, e) = 85$ AU, 0.59)] and not plotted. (Orbital elements computed by B. G. Marsden.)
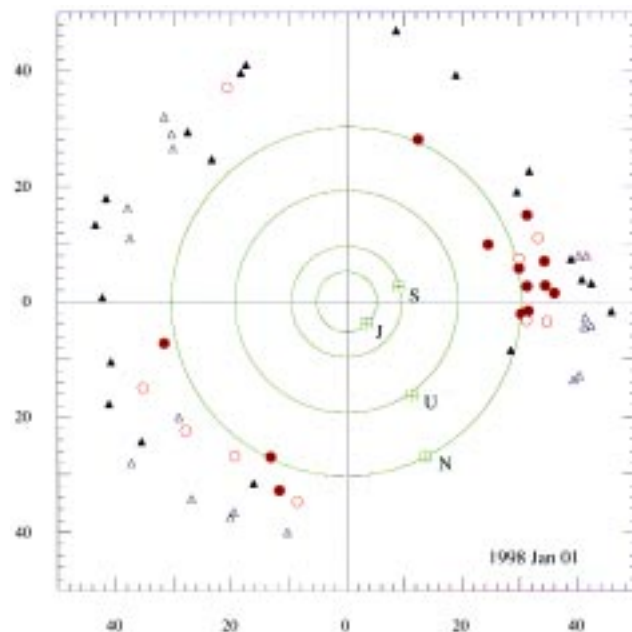

FIG. 3.—Plan view of the solar system on 1998 January 1. Plutinos are shown as circles, all other KBOs as triangles. The orbits and positions of the gas-giant planets are marked. Filled and open symbols denote multi- and single-opposition orbits, respectively. Ecliptic longitude 0° is to the right and increases counterclockwise.

TABLE 2

PHOTOMETRY

Name	ID	Dates	R^a (AU)	Δ^a (AU)	α^a (deg)	$m_R \pm \sigma(N)^b$	H^c	D^d (km)
1996 TL$_{66}$......	3079.2	1996 Oct 9, 12	35.23	34.30	0.6	20.60 ± 0.04 (5)	5.01	550
1996 TO$_{66}$	6015.7	1996 Oct 12, 13	45.67	44.70	0.3	21.00 ± 0.05 (6)	4.38	759
1996 TP$_{66}$.......	5058.2	1996 Oct 11, 13	26.49	25.51	0.4	21.06 ± 0.04 (6)	6.82	246
1996 TQ$_{66}$	1073.4	1996 Oct 8, 12	34.62	33.65	0.4	22.28 ± 0.05 (8)	6.86	242
1996 TR$_{66}$	2050.0	1996 Oct 8, 12	35.96	34.97	0.3	22.65 ± 0.09 (6)	7.08	219
1996 TS$_{66}$	6079.7	1996 Oct 12, 14	38.96	38.06	0.6	21.84 ± 0.07 (6)	5.87	382
1997 CQ$_{29}$	5111.0	1977 Feb 4, 7, 9	41.16	40.24	0.5	22.58 ± 0.08 (6)	6.38	301
1997 CR$_{29}$	4087.0	1997 Feb 3, 7, 9	42.00	41.01	0.1	22.98 ± 0.02 (5)	6.76	253
1997 CS$_{29}$	4032.4	1997 Feb 3, 6, 9	43.62	42.70	0.5	21.37 ± 0.10 (4)	4.92	592
1997 CT$_{29}$	3083.1	1997 Feb 2, 4, 7	44.97	43.98	0.0	23.14 ± 0.28 (5)	6.66	266
1997 CU$_{29}$	7021.6	1997 Feb 6, 7, 9	44.57	43.66	0.5	22.78 ± 0.02 (6)	6.23	323
1997 CV$_{29}$	7079.6	1997 Feb 6, 7, 9	40.09	39.11	0.1	22.95 ± 0.12 (8)	6.94	234
1997 CW$_{29}$......	9035.3	1997 Feb 8	42.48	41.53	0.4	22.43 ± 0.15 (2)	6.11	342

[a] Heliocentric distance, geocentric distance, and phase angle at the time of discovery, respectively.

[b] Here m_R = apparent red magnitude, σ = standard deviation of the mean, and N = number of measurements. An additional nonrandom uncertainty of order 0.2 mag must be added to the listed error to account for the unknown color of each KBO.

[c] Absolute magnitude computed from m_R using H-G relation from Bowell et al. 1989.

[d] Effective diameter computed assuming red geometric albedo $p = 0.04$.

TABLE 3

SKY-PLANE SURFACE DENSITIES FROM THE 8K CCD SURVEY

$m_R{}^a$	N^b	f^c	$N/(fA)^d$ (deg^{-2})	Σ^e (deg^{-2})
20.5 ± 0.25......	1	0.85 ± 0.02	0.023	0.023 ± 0.023
21.0 ± 0.25......	2	0.80 ± 0.02	0.049	0.072 ± 0.042
21.5 ± 0.25......	1	0.70 ± 0.02	0.028	0.100 ± 0.050
22.0 ± 0.25......	1	0.60 ± 0.03	0.032	0.132 ± 0.059
22.5 ± 0.25......	4	0.50 ± 0.04	0.181	0.31 ± 0.10
23.0 ± 0.25......	4	0.13 ± 0.05	0.597	0.91 ± 0.43

[a] Apparent red limiting magnitude and bin width.

[b] Number of objects.

[c] Detection efficiency and its statistical uncertainty (Fig. 1).

[d] Differential surface density computed using $A = 51.5$ deg^2.

[e] Cumulative sky-plane surface density. The errors were calculated from a combination of Poisson uncertainties and uncertainties in the estimated detection efficiency.

TABLE 4

OTHER SURFACE DENSITY CONSTRAINTS

m_R	Area (deg^2)	N	$\Sigma_{TN}{}^a$ (deg^{-2})	Reference
CCD surveys:				
22.0[b]......	4.9	0	≤ 1.1	1
23.2.......	9.5	14	1.5 ± 0.5	2
23.5.......	0.7	2	$2.9^{+2.9}_{-2.4}$	3
24.2.......	5.1	17	3.9 ± 1.1	2
24.8	1.2	7	$5.8^{+3.3}_{-2.9}$	4
Photographic surveys:				
16.8.......	1530	1	6.5×10^{-4}	5
19.5[c]......	6400	0	$<8.6 \times 10^{-4}$	6
20.0.......	297	0	$<1.9 \times 10^{-2}$	7

NOTE.—Adapted from Jewitt et al. 1996.

[a] Upper limits are 99.9% (approximately 3 σ) confidence limits.

[b] Calculated from quoted limiting $m_V = 22.5$, using $V - R = 0.5$.

[c] Calculated from quoted limiting $m_V = 20.0$, using $V - R = 0.5$.

REFERENCES.—(1) Levison & Duncan 1990; (2) Jewitt et al. 1996; (3) Irwin et al. 1995; (4) Jewitt & Luu 1995; (5) Tombaugh 1961; (6) Kowal 1989; (7) Luu & Jewitt 1988.

cance, we omit the Cochran et al. datum from the following analysis.

3.1. Luminosity Function

We plot the luminosity function of the KBOs in Figure 4. Error bars in the figure assume Poisson counting statistics. The surface densities derived from the 8K survey smoothly match surface densities of fainter objects determined earlier (Jewitt & Luu 1995; Jewitt et al. 1996; Irwin et al. 1995). This agreement provides compelling evidence that the efficiencies of the various ground-based surveys have been accurately established. We fit the cumulative surface density, $\Sigma(m_R)$, with weighted power law fits of the form

$$\log \Sigma(m_R) = \alpha(m_R - m_0) , \qquad (1)$$

where m_0 is the magnitude at which $\Sigma = 1$ deg^{-2} is reached, while 10^α gives the slope of the luminosity function. A fit to
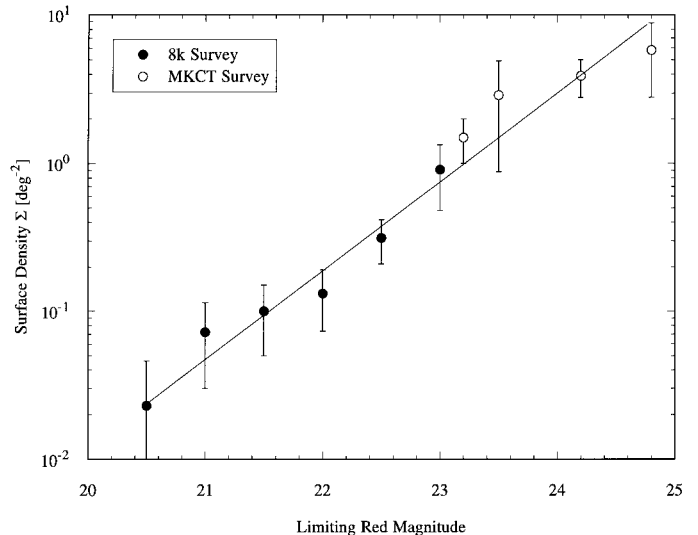

FIG. 4.—Luminosity function of the Kuiper Belt determined exclusively from CCD observations at red magnitudes $m_R > 20$. The point at $m_R = 23.5$ is from Irwin, Tremaine, & Żytkow (1995). All others are from the MKCT survey (Jewitt, Luu, & Chen 1996) and the present work. The diagonal line is a weighted least-squares fit to the data (eq. [1]).

the published data with $m_R \geq 23$ yields $\alpha = 0.38 \pm 0.14$ and $m_0 = 22.67 \pm 0.51$. A fit to the new data alone ($m_R < 23$) yields $\alpha = 0.56 \pm 0.15$ and $m_0 = 23.37 \pm 0.37$. The slopes and zero points are both formally consistent, so we combine the data and obtain

$$\alpha = 0.58 \pm 0.05 , \quad m_0 = 23.27 \pm 0.11 \quad (20 \leq m_R \leq 25) .$$
(2)

Evidently, the surface density increases by a factor of $10^\alpha \approx 4$ per magnitude in this range. Equation (2) is consistent with published upper limits to the surface density of the Kuiper Belt obtained from CCDs (cf. Luu & Jewitt 1988; Levison & Duncan 1990; Gladman & Kavelaars 1997).

3.2. Size Distribution

One of the most fundamental issues concerns the size distribution of the Kuiper Belt objects. The size distribution is a product of the accretion history of KBOs, perhaps modified by the effects of collisions (Farinella & Davis 1996). The luminosity function provides only an indirect measure of the size distribution of the KBOs because of the effects of observational selection (Jewitt & Luu 1995; Irwin et al. 1995). Flux-limited (as opposed to volume-limited) surveys of the present kind are biased toward large, nearby, high-albedo KBOs at the expense of their smaller, darker, more distant cousins. To extract the size distribution from the luminosity function, we use Monte Carlo models to simulate the survey and, necessarily, make assumptions about the geometric albedos and distance distributions of the KBOs.

3.2.1. Albedo Distribution

There are no measurements of the albedos of KBOs. The nuclei of short-period comets and the Centaurs are believed to have been recently dislodged from the Kuiper Belt (Duncan, Quinn, & Tremaine 1988), and so they may provide our best, albeit indirect, indicators of KBO albedos. The red geometric albedos of the nuclei of comets are typically $p_R \sim 0.04$ (see references in Jewitt 1996). Thermal emission from the Centaurs 5145 Pholus and 2060 Chiron has been used to derive $p_R \approx 0.04$ (Davies et al. 1993) and $p_R = 0.13^{+0.04}_{-0.03}$ (Campins et al. 1994; Altenhoff & Stumpff 1995), respectively. The derived albedo of Chiron may be elevated by coma contamination of the scattered light. In any event, it appears that both Centaurs have dark surfaces.

For the models discussed below, we have assumed a red geometric albedo, $p_R = 0.04$, throughout. Diameters listed for this albedo in Table 2 may be rescaled to other albedos, p, by multiplying by $(0.04/p)^{1/2}$. It is possible that the albedo is a systematic function of the size of the KBO (Jewitt & Luu 1998). This would be the case, for example, if surface frosts were deposited from weakly bound atmospheres of the largest KBOs. This is the origin of 2300 km diameter Pluto's high albedo ($p_R = 0.60$; Albrecht et al. 1994), and it is possible that other large KBOs are similarly reflective.

Different surface types in the Kuiper Belt are suggested by the observation of pronounced color differences at optical (Luu & Jewitt 1996) and near-infrared (Jewitt & Luu 1998) wavelengths. In any event, we also considered models in which the geometric albedo ramps from 0.04 at radius 50 km to 0.6 at radius 1000 km, our intent being to examine the sensitivity of the results to the assumed form of the albedo. In general, we found that the rather extreme difference in adopted albedo functions resulted in only small differences in the derived quantities, as we note below. Essentially, this is because the flux scattered from a KBO is proportional to $p_R r^2/R^4$ and so is more sensitive to variations in radius, r, and heliocentric distance, R, than in albedo.

3.2.2. Distance Distribution

The Monte Carlo model includes both classical KBOs and Plutinos. The SKBOs are neglected since these are less common in the data than either classical KBOs or Plutinos, and their orbital distributions are presently uncertain. Both classes of object are assumed to obey differential power-law radius distributions of the form $n(r)dr = \Gamma r^{-q} dr$, where $n(r)dr$ is the number of objects with radii in the range r to $r + dr$ and Γ and q are constants. Radius takes values in the range $r_{min} \leq r \leq r_{max}$. In each model, r_{min} is set equal to the radius of the faintest body that can be detected when at perihelion. For example, at perihelion distance 26 AU and with magnitude 23, we find $r_{min} = 46$ km. The maximum radius r_{max}, is treated as a parameter of the model to be constrained observationally. We implicitly assume that the size distributions and albedos of classical KBOs and Plutinos are identical. We require the numerical simulations to reproduce the distribution of heliocentric distances of KBOs at discovery, and to fit the apparent ratio of Plutinos to classical Kuiper Belt objects ($\approx 35\%$; Fig. 2).

For each model KBO, we used a random-number generator to select values of semimajor axis and eccentricity from distributions (see Table 5). We then computed instantaneous heliocentric distances of the model KBOs at random times within each orbit. We confirmed that the resulting distribution of heliocentric distances obeyed Kepler's "equal areas in equal times" law. For simplicity, all objects were taken to have zero inclination. This should not introduce a bias in the interpretation of the luminosity function unless the inclination distribution is a function of KBO size (a possibility for which the observational data provide no support). For the distribution of semimajor axes in the classical Kuiper Belt, we assumed a modified power-law variation, $n(a)da = n(a_{min})(a_{min}/a)^p f(a)da$, in the range $a_{min} \leq a \leq a_{max}$ (Table 5). Prompted by the apparent distribution of semimajor axes (Fig. 2), and following numerical exploration of both larger and smaller values, we adopted $a_{min} = 42$ AU and $a_{max} = 50$ AU for most models. Models with $a_{min} < 42$ AU strongly violate the observed deficiency of objects with small semimajor axes (Fig. 2). Models with $a_{max} > 50$ AU generally fit the slope of the luminosity func-

TABLE 5
DISTRIBUTIONS USED IN THE MODEL

Quantity	Classical KBOs	Plutinos
Radius ($r_{min} \leq r \leq r_{max}$)	$n(r)dr = \Gamma r^{-q} dr$	$n(r)dr = \Gamma r^{-q} dr$
Semimajor axis ($a_{min} \leq a \leq a_{max}$)......	$n(a)da = n(a_{min})(a_{min}/a)^p f(a)da$	$n(a)da = \delta(39.4)$
Eccentricity ($0 \leq e \leq e_{max}$)	$n(e)de = \exp(-e^2/2\sigma_c^2)de$	$n(e)de = \exp[-(e - e_0)^2/2\sigma_P^2]de$

tion as well as the models presented here. However, as discussed in § 3.6, these models contradict the empirical absence of KBOs with $a_{max} > 50$ AU. We found the results of the models to be a weak function of radial index p in the range $1 \leq p \leq 3$. The results presented here all assume $p = 2$ and $a_{max} = 50$ AU.

We considered two cases for the dimensionless function $f(a)$:

$$f(a) = 1 , \tag{3}$$

$$f(a) = 1 - \exp\left[\frac{-(a - a_{min})}{15}\right] \tag{4}$$

(see Table 5). The first case corresponds to a pure power-law surface density gradient such as that presumed to exist in the preplanetary solar nebula, while the second was used to represent the depletion of KBOs in orbits near Neptune owing to gravitational "sculpting" by that planet (Holman & Wisdom 1993; Duncan et al. 1995). Again, prompted by the observations (Fig. 2), the eccentricity distribution in the classical Kuiper Belt was taken to be Gaussian with mean $e_0 = 0$ and standard deviation $\sigma_c = 0.06$ (FWHM = 0.15) up to maximum $e_{max} = 0.25$. The distribution of Plutinos was represented in the models by a set of objects with semimajor axes $a_{3:2} = 39.4$ AU and a Gaussian eccentricity distribution with mean $e_0 = 0.1$ and standard deviation $\sigma_P = 0.13$ (FWHM = 0.33) (cf. Malhotra 1996) truncated at $e = 0$ and $e_{max} = 0.4$.

Sample models with $p = 2$ and $q = 3, 4, 5$ and normalized to unity at $m_R = m_0$ are shown in Figure 5. The models have $r_{max} = 2000$ km and are insensitive to r_{min}. We employed equation (4) but observed that alternate models using equation (3) yielded nearly identical results. With these caveats, the best-fit size distribution has

$$q = 4.0 \pm 0.5 \tag{5}$$

where we have quoted our best guess as to the uncertainty. The index is larger than we previously believed ($q \approx 3$) based on more limited survey data in the fainter magnitude
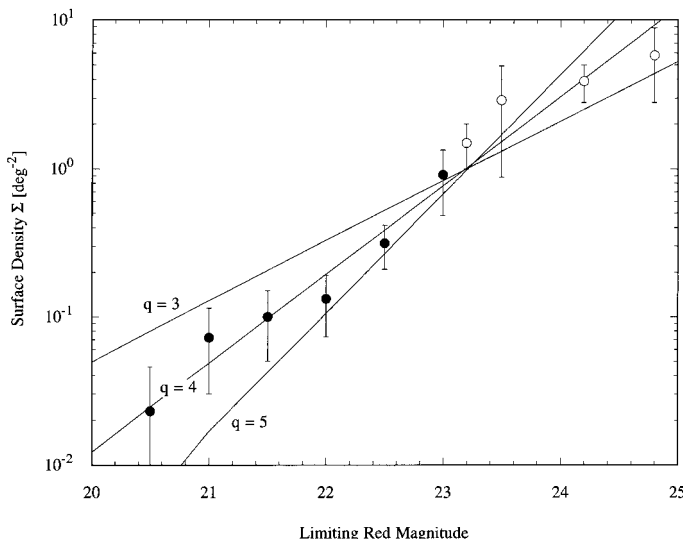
range $23.0 \leq m_R \leq 24.8$ (Jewitt et al. 1996). Equation (5) is established from data in the $20 \leq m_R \leq 25$ magnitude range (i.e., neglecting all photographic data). The increased span of the data in Figure 5 over that previously available gives us greater confidence in the derived size distribution index. Incorporation of the aforementioned albedo-size relation (§ 3.2.1) increases q by about 0.5. Within the uncertainties, both observational and due to modeling, the size distribution index in the Kuiper Belt is compatible with $q \approx 3.5$, expected from a purely collisional production function (Dohnanyi 1969), but also with $q \approx 4.5$, predicted by aggregation models (Yamamoto & Kozasa 1988). There is no physical reason why a single power law should describe the size distribution at all radii. The luminosity function outside the $20 \leq m_R \leq 25$ range may differ, and awaits observational determination. It has been remarked that collisional modification should cause a flattening of the distribution function at smaller radii (Farinella & Davis 1996); the available data are not of quality sufficient to show such an effect.

3.3. Upper Size Cutoff

Some current models assert that the Kuiper Belt is a region of the preplanetary disk in which planetesimal growth was prematurely arrested by the sudden birth of Neptune (e.g., Bailey 1994). In this picture, the KBOs grow concurrently with Neptune, and the sizes of the largest KBOs provide a measure of the timescale on which Neptune grew (see, e.g., Stern & Colwell 1997; Kenyon & Luu 1998). Massive planetesimals scattered into the Kuiper Belt by Neptune might also have terminated growth by pumping the local velocity dispersion (Morbidelli & Valsecchi 1997). We are interested in searching for evidence of an effective maximum size among the KBOs, which would appear in our data as a downturn in the bright end of the luminosity function.

Figure 6 shows the data together with $q = 4$ power-law models truncated at $r_{max} = 250, 500, 1000,$ and 2000 km. The data are well matched by all models except that with $r_{max} = 250$ km, which clearly underestimates the number of objects brighter than $m_R = 22$. We conclude that there is no evidence in the present CCD data for an upper limit to the
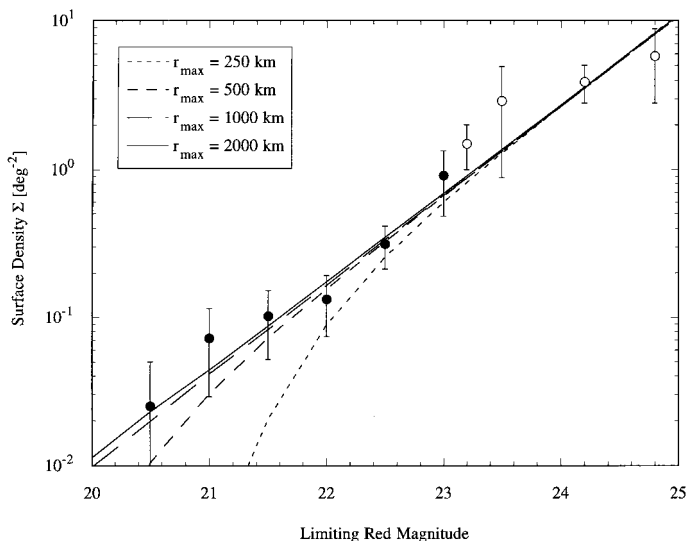

FIG. 5.—Monte Carlo models as described in the text. Power-law size distributions with indices $q = 3$, 4, and 5 are marked. All models have $p = 2$, $r_{max} = 2000$ km, and $r_{min} \ll r_{max}$ and are normalized to unity at $m_R = m_0$. The apparent Plutino fraction for these models is 35%. The classical Kuiper Belt is taken to extend from 40 to 50 AU.

FIG. 6.—Power-law size distributions with $q = 4$ truncated at $r_{max} = 2000, 1000, 500,$ and 250 km. The curves with $r_{max} > 250$ km all fit the data.

radii of KBOs, such as might result from a period of growth limited by the emergence of nearby Neptune. If such a limit exists, the CCD data only constrain it to occur at a radius $r_{max} > 250$ km. This conclusion is compatible with the 2300 km diameter of the largest known KBO, Pluto.

The mass of a $q = 4$ power-law distribution of spherical bodies is $M = 4\pi\rho N r_{min}^3 \ln(r_{max}/r_{min})$, where the bulk density is here taken to be $\rho = 2000$ kg m^{-3} and N is the number of bodies with radii in the range $r_{min} \leq r \leq r_{max}$. The number of objects in the 30 AU $\leq R \leq$ 50 AU heliocentric distance range and larger than $r_{min} = 50$ km is $N \sim 7 \times 10^4$ (Jewitt et al. 1996). With $r_{max} = 1150$ km (the radius of Pluto), we obtain $M = 6.8 \times 10^{23}$ kg ($0.12 M_E$, where the mass of Earth is $M_E = 6 \times 10^{24}$ kg). If we instead adopt $r_{min} = 1$ km, to account for KBOs too small to be detected in the ground-based surveys, we obtain $M = 1.6 \times 10^{24}$ kg ($0.26 M_E$). These masses are compatible with our previous estimates obtained using more limited data (Jewitt et al. 1996).

3.4. Plutino Fraction

Thirteen of the 34 multiopposition KBOs (including Pluto) reside in the 3:2 resonance ($a_{3:2} = 39.4$ AU), yielding an *apparent* Plutino fraction $P_a = 13/34 \approx 0.38$ (see Table 6). This fraction persists when we count orbits of all qualities ($P_a = 21/61 \approx 0.34$). However, we expect that the apparent Plutino fraction is enhanced relative to the *intrinsic* Plutino fraction, P_i, because of the effects of observational bias. There are at least three potential sources of such bias. First, the Plutinos have smaller semimajor axes than most other known KBOs (Fig. 2). For this reason they are discovered at systematically smaller heliocentric distances (Fig. 3), where they are brighter, more readily detected, and therefore overrepresented in the data. Second, the Plutinos are aphelion librators that reach perihelion, and are most easily observed, when near $\pm 90°$ from Neptune (Malhotra 1996). Figure 7 shows P_a versus ecliptic longitude. Directions toward Neptune have not been observed, as a result of the proximity of the Milky Way. A concentration along directions $\sim 90°$ from Neptune is evident, as expected of 3:2 aphelion librators. The degree to which this azimuthal variation causes a bias in the data depends on the azimuthal distribution of observing directions in past KBO surveys. Our own surveys (e.g., Jewitt & Luu 1995; Jewitt et al. 1996)
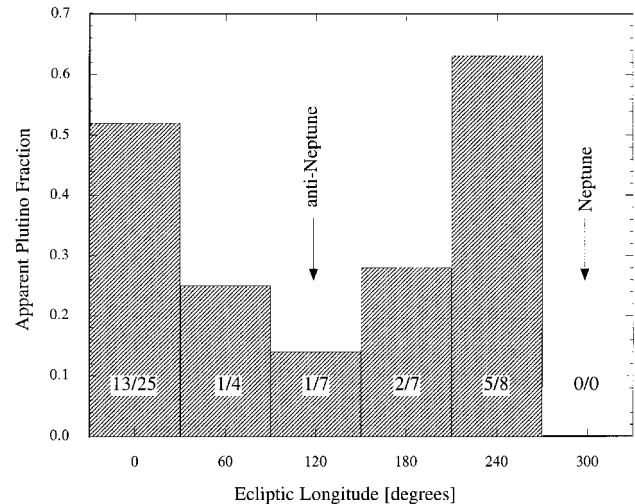

Fig. 7.—Distribution of the apparent Plutino fraction with ecliptic longitude, extracted from Fig. 3. The numbers of Plutinos and other KBOs are marked within each histogram bin. The ecliptic longitudes of Neptune and the anti-Neptune direction are marked.

have been concentrated in the sectors $\pm 90°$ from Neptune, thus tending to elevate P_a above P_i. A third bias, which acts in the opposite sense, results from the argument-of-perihelion libration, which maintains Pluto's perihelion at high ecliptic latitude ($16°$). It is not known whether the Plutinos as a whole share the libration. If they do, the concentration of past surveys in directions toward the ecliptic could produce an underestimate of the number of resonant objects.

Monte Carlo simulations allow us to estimate an upper limit to the intrinsic Plutino fraction, P_i, needed to produce the apparent P_a. We represent the two components of the Kuiper Belt by orbital distributions as in Table 5, with $f(a)$ given by equation (4). The model parameters are adjusted to match the observed $P_a \approx 0.35$. Under these conditions, and with $r_{max} = 1000$ km, we find $P_i(q = 3) = 0.22$, $P_i(q = 4) = 0.17$, and $P_i(q = 5) = 0.12$. The Plutinos are overrepresented in flux-limited surveys by a factor $P_a/P_i \approx 1.6$–2.9. With $r_{max} = 250$ km, we obtain $P_i(q = 3) = 0.18$, $P_i(q = 4) = 0.14$, and $P_i(q = 5) = 0.11$ ($P_a/P_i \approx 1.9$–3.2). It thus appears that the Plutinos are overrepresented in the observational data

TABLE 6

ORBITAL PARAMETERS OF MULTIOPPOSITION 3:2 RESONANCE OBJECTS

Object	q (AU)	Q (AU)	Epoch	M (deg)	ω (deg)	Node (deg)	i (deg)	e	a (AU)	Opp.[a]	Reference[b]	Discovery Date
1996 TP$_{66}$	26.38	53.05	1997 Dec 18	357.0	74.6	316.6	5.7	0.336	39.712	2	MPC 30690	1996 Oct 11
1993 SB	26.91	52.18	1997 Dec 18	324.4	77.9	354.8	1.9	0.319	39.549	4	MPC 28317	1993 Sep 16
1994 TB	27.05	52.63	1997 Dec 18	330.3	98.0	317.3	12.1	0.321	39.842	4	MPC 30292	1994 Oct 2
1995 HM$_5$	29.48	49.26	1997 Dec 18	325.5	61.1	186.7	4.8	0.251	39.369	3	MPC 30093	1995 Apr 26
1996 SZ$_4$	29.57	50.07	1997 Dec 18	342.8	26.9	16.0	4.7	0.257	39.817	2	MPC 30785	1996 Sep 16
Pluto	29.68	49.54	1997 Jun 1	10.6	114.4	110.4	17.1	0.251	39.611	66	DE403	1930 Feb 18
1995 YY$_3$	30.70	48.08	1997 Dec 18	4.5	320.8	99.8	0.4	0.221	39.389	2	MPC 27920	1995 Dec 24
1993 RO	31.48	47.73	1997 Dec 18	0.6	188.1	170.3	3.7	0.205	39.608	4	MPC 30688	1993 Sep 14
1993 SC	32.24	47.52	1997 Dec 18	37.6	318.4	354.6	5.1	0.192	39.882	4	MPC 30092	1993 Sep 17
1996 RR$_{20}$	32.55	47.55	1997 Dec 18	107.2	54.5	163.5	5.3	0.187	40.051	2	MPC 30690	1996 Sep 15
1995 QZ$_9$	33.70	45.85	1997 Dec 18	31.5	143.8	188.0	19.5	0.153	39.770	3	MPC 30689	1995 Aug 29
1996 TQ$_{66}$	34.59	44.71	1997 Dec 18	356.6	22.2	10.7	14.6	0.128	39.651	2	MPC 30690	1996 Oct 8
1994 JR$_1$	34.76	44.11	1997 Dec 18	1.5	103.5	144.9	3.8	0.119	39.434	3	MPC 30291	1994 May 12

NOTE.—Orbital parameters from B. G. Marsden.
[a] Number of oppositions at which the object has been observed.
[b] (MPC) Minor Planet Circular; (DE403) Standish et al. 1995.

by a factor that is uncertain but is of order 1.5–3. This overrepresentation applies only for a Kuiper Belt truncated at 50 AU (the practical limit of the published surveys). If the Kuiper Belt extends much beyond 50 AU, the intrinsic Plutino fraction could shrink substantially. Likewise, smaller values of r_{max} would lead to smaller P_i and to larger values of the bias factor, but $r_{max} < 250$ km appears to be unlikely from the shape of the luminosity function (§ 3.3). We conclude that the Plutinos constitute only ~10%–20% of the KBOs in the 30–50 AU region. In view of the heterogeneous nature of the observational data (e.g., only half the objects in Figs. 2, 3, and 7 were detected in systematic surveys with well-defined [and published] limiting magnitudes and areal coverage), it is probably not yet worthwhile to attempt a more exact estimate.

3.5. Relative Populations of the 3:2 and 2:1 Resonances

The resonance-sweeping hypothesis predicts that the populations of the 3:2 and 2:1 resonances should be in the ratio $n_{2:1}/n_{3:2} \approx 1$ (Malhotra 1995). None of the 34 multi-opposition objects reside in the 2:1 resonance ($a_{2:1} = 47.6$ AU), compared with 13 (including Pluto) in the 3:2 resonance, for an apparent ratio $n_{2:1}/n_{3:2} \approx 0/13$ (see Fig. 2). Could this apparent deficit of 2:1 resonant objects be a result of observational selection, or does it represent a failure of the resonance-sweeping hypothesis? For objects of a given size, the magnitude difference resulting from the greater distance of the 2:1 resonance is a modest $\Delta m_R = 10$ log $(a_{2:1}/a_{3:2}) = 0.8$ mag. From equation (1), this would produce an apparent ratio $n_{2:1}/n_{3:2} = 10^{-\alpha \Delta m_R} = \frac{1}{3}$ ($\alpha = 0.6$; see § 3.1) if the two resonances are equally populated. From the 13 multiopposition objects in the 3:2 resonance, we would expect to have recorded $13/3 \approx 4$ in the 2:1 resonance, but instead we have zero.

We examine this issue in more detail by using our bias model to account for the distribution of eccentricities of resonant KBOs, and to examine the effect of a possible upper size cutoff. We divided 10^5 KBOs equally into the 3:2 and 2:1 resonances and then used the bias model to determine the observability of the objects as a function of magnitude and size distribution. The result is a "bias correction factor,"

$$b(q, r_{max}) = \frac{(n_{2:1}/n_{3:2})_{apparent}}{(n_{2:1}/n_{3:2})_{intrinsic}}, \quad (6)$$

which we have listed in Table 7 for several values of q and r_{max} (so as to illustrate the sensitivity of the bias to these parameters). For the canonical case, we find $b(4, 1000) \approx 0.3$, roughly independent of magnitude and

close to the analytic estimate above. From the 13 multi-opposition objects in the 3:2 resonance we would expect to have detected about four multiopposition objects in the 2:1 resonance (Figure 8). By Poisson statistics, the probability that we might have detected no objects when the mean is 4 is $P(0, 4) = 1.8\%$, so that we can reject the hypothesis that the 2:1 and 3:2 resonances are equally populated at the 98.2% (~2.5 σ) level. However, a formal (3 $\sigma = 99.7\%$) rejection of the hypothesis is not possible based on the available data. A 3 σ rejection would require an additional four objects in the 3:2 resonance (and none in the 2:1). We note that among the single-opposition orbits there are a further nine KBOs with elements in the vicinity of the 3:2 resonance but there are no candidate 2:1 objects. For this reason, we expect that more stringent constraints on the intrinsic resonance population ratio will emerge as the orbits of known KBOs are refined by new astrometry, and as new KBOs are discovered by future surveys.

In summary, while the data provide no evidence that the 2:1 resonance is populated at all, we cannot (yet) formally disprove the hypothesis that the 2:1 and 3:2 resonances are equally populated. The measured population ratios are thus formally consistent with the most basic prediction of the resonance-sweeping hypothesis by Malhotra (1995). The newly recognized low abundance of the 3:2 Plutinos is also consistent with at least some of the resonance-sweeping simulations (see, e.g., Fig. 3 of Malhotra 1995, in which ~13% of the surviving objects are Plutinos). In view of the fact that the published resonance-sweeping simulations neglect several effects likely to be of importance (e.g., stochastic jumps in the migration of Neptune due to impulsive ejection of massive planetesimals), we must conclude that the model and data are in reasonable agreement. An alternative model in which the structure of the Kuiper Belt is largely set by massive, runaway Neptune-scattered planetesimals (Morbidelli & Valsecchi 1997) makes no quantitative predictions of the Plutino fraction and so cannot be tested with our new survey data.

3.6. Radial Extent of the Classical Kuiper Belt

The known KBOs were all discovered in a relatively narrow range of heliocentric distances (26 AU $\leq R \leq$ 46

TABLE 7

BIAS CORRECTION FACTOR

q	21.0	21.5	22.0	23.0	24.0	25.0
$r_{max} = 250$ km:						
3.5	...	0.047	0.104	0.298	0.347	0.369
4.0	...	0.044	0.097	0.254	0.292	0.305
4.5	...	0.042	0.089	0.218	0.245	0.256
$r_{max} = 1000$ km:						
3.5	0.346	0.368	0.370	0.376	0.375	0.376
4.0	0.298	0.304	0.306	0.310	0.310	0.308
4.5	0.247	0.250	0.251	0.254	0.255	0.256

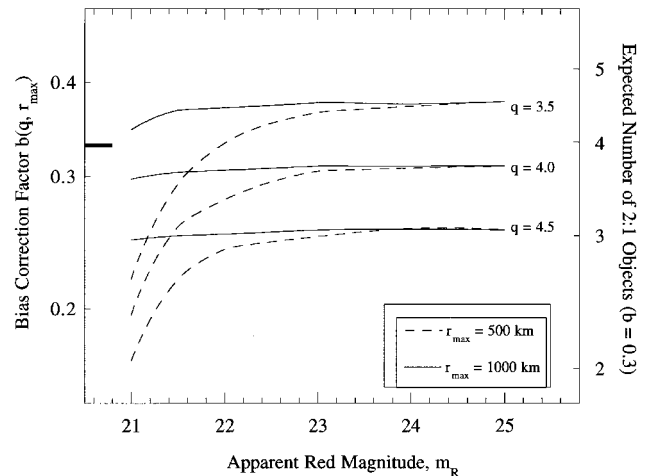NOTE.—Listed is $b(q, r_{max})$ (eq. [6]) for limiting red magnitudes $m_R = 21.0$–25.0.

FIG. 8.—Bias correction factor, $b(q, r_{max})$, calculated from Monte Carlo simulations of the 3:2 and 2:1 resonant objects. Results for three values of the size distribution index are shown. The thick horizontal bar marks the bias estimated analytically in the text. The sharp decrease in $b(q, 500)$ at $m_R \leq 22$ occurs because some of the largest objects in this distribution are invisible at the 2:1 resonance.

AU) and, with the exception of 1996 TL_{66} ($a = 85$ AU), have a similarly restricted range of semimajor axes. In this section we ask to what extent the observations can be used to constrain the population of KBOs that have semimajor axes much larger than those observed. We focus our attention on the numerically dominant members of the classical Kuiper Belt. A similar analysis of the TL_{66}-class scattered KBOs will be possible once more of these objects have been identified.

We considered models in which the semimajor axes of classical Kuiper Belt objects were distributed as power laws in the range $42 \leq a \leq a_{max}$. The eccentricities were matched to those of the 42 AU $\leq a \leq 46$ AU region (Fig. 2; cf. Table 5, with $e_{max} = 0.12$). The size distribution was taken to be a $q = 4$ power law (§ 3.2) in the radius range $r_{min} \leq r \leq r_{max}$, and a uniform 0.04 albedo was assumed. Plutinos were added according to the prescription outlined in §§ 3.4 and 3.5, and each model was required to generate an apparent Plutino fraction $P_a \sim 0.35$ to be consistent with the observations. We simulated the three most productive surveys (Jewitt & Luu 1995; Jewitt et al. 1996, and the present 8K survey) by taking proper account of the detection efficiency as a function of apparent magnitude. The different surveys yielded similar constraints, and so we confine our attention here to the simulations of the 8K survey.

The main result is that power-law disks with outer radii much larger than 47 AU predict apparent radial distributions of objects that are quite different from those observed. This is illustrated in Figure 9, where we compare simulations having $a_{max} = 47$ AU and $a_{max} = 200$ AU (parameters in common to the two simulations are listed in the legend to the figure). The latter simulation yields a large number ($\sim 40\%$) of KBOs at discovery distances $R \geq 50$ AU, whereas in the observational sample there are none. This discrepancy remains for any plausible size distribution and radial distribution indices, provided $a_{max} > 47$ AU. We note that Dones (1997) already examined the Jewitt et al. (1996) survey and reached an essentially identical conclusion.

How can this result be understood? One possibility is that the survey is insensitive to the more distant objects because of their lower sky-plane velocities. However, Monte Carlo simulations (§ 2) of objects moving at rates down to $2'' \ hr^{-1}$ (corresponding to $R \approx 70$ AU) showed no loss of efficiency at even the lowest rates. We therefore reject the possibility that the absence of more distant objects is an artifact of the survey. Another possibility is that the maximum object size is a decreasing function of semimajor axis. This type of variation would seem to be physically plausible, as a consequence of the radial density gradient and the longer timescales for growth in the outer parts of the preplanetary disk. We recomputed Monte Carlo simulations including this effect and, indeed, achieved a better match to the survey data. However, the rate of decrease of r_{max} required to obtain a match is very large and seems to us implausible. Indeed, the surface density in a $p = 2$ disk at 45 AU (where we see many objects) is only 50% larger than at 55 AU (where we see none), and it is hard to imagine that r_{max} could be so sensitive to the local surface density. It is worth noting that the distribution and sizes of the known KBOs provide no evidence that r_{max} decreases with a. The third possibility is that the Kuiper Belt surface density does not follow a simple power-law variation at distances beyond the observed region. In fact, our data are consistent with the presence of a discrete outer edge to the belt at
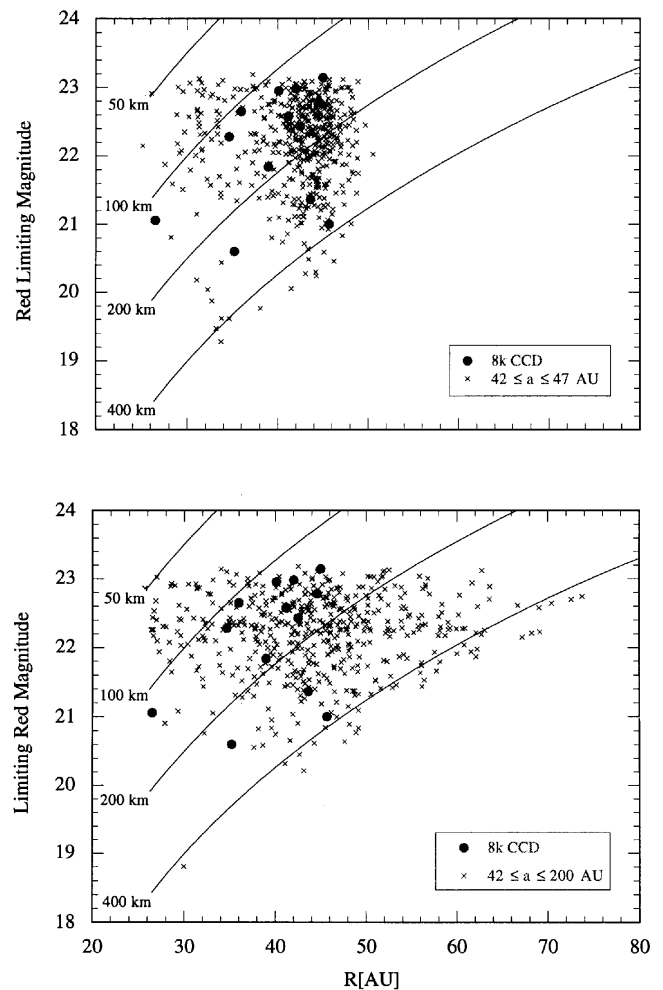

FIG. 9.—Heliocentric distance at discovery vs. apparent red magnitude. Filled circles mark objects found in the 8K survey. Crosses denote simulated objects that passed the survey detection criteria. The results of two models are shown: *Top*, the classical Kuiper Belt is taken to extend to maximum semimajor axis $a_{max} = 47$ AU; *bottom*, $a_{max} = 200$ AU. In both models, the KBOs obey a power-law size distribution with index $q = 4.0$, and all have albedo $p_R = 0.04$. Plutinos have been included in proportions needed to yield an apparent Plutino fraction $P_a \approx 0.35$. The radial density index in the classical Kuiper Belt is taken to be $p = 2$ in both models, and in the particular simulation shown here we have chosen $r_{max} = 500$ km. Diagonal lines show the apparent magnitude as a function of heliocentric distance for KBO radii 50, 100, 200, and 400 km.

$a = 47$ AU. We are uncomfortable with the notion that the Kuiper Belt might have an edge near 50 AU (what physical process could be responsible?), but our data nevertheless suggest this as a possibility. Most likely, we expect that some combination of a radial decrease in r_{max} and a steepening of the Kuiper Belt surface density at about 45–50 AU operates to yield the observed radial distribution. We hope to distinguish among these possibilities, and to probe more distant regions of the Kuiper Belt, by further deep imaging observations.

3.7. *Photographic Constraints*

Finally, we examine the effect of including photographic survey results on the conclusions reached above from CCD data alone. The photographic and CCD data are plotted together in Figure 10. Also plotted are the truncated $q = 4$ models from Figure 6. The Tombaugh (1961) and Luu & Jewitt (1988) photographic surveys are compatible with extrapolations of equations (1) and (2) to $m_R = 16$ (i.e., no
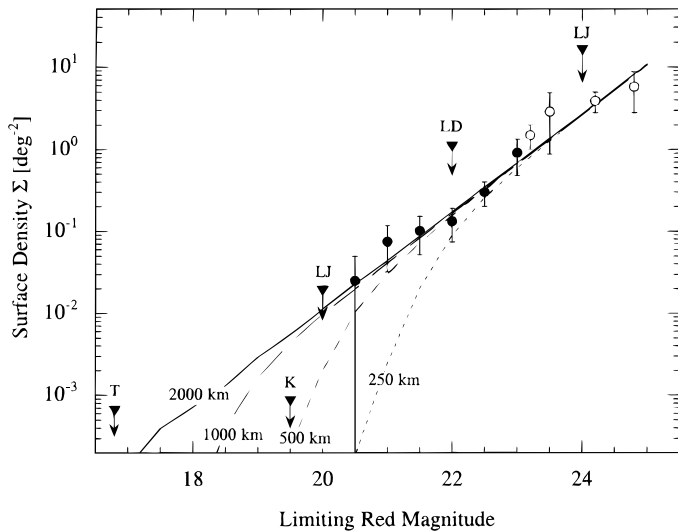
FIG. 10.—Luminosity function of the Kuiper Belt including photographic survey constraints at $m_R \leq 20$. "LJ" = Luu & Jewitt (1988), "LD" = Levison & Duncan (1990), "K" = Kowal (1989), and "T" = Tombaugh (1961). Truncated $q = 4$ power-law size distribution models are marked.

1. The Kuiper Belt luminosity function is well defined in the red magnitude range $20 \leq m_R \leq 25$, with slope $a = 0.58 \pm 0.05$. The cumulative surface density of Kuiper Belt objects reaches 1 deg^2 at $m_R = 23.3 \pm 0.1$.

2. The slope of the luminosity function is reproduced by Monte Carlo simulations in which the Kuiper Belt objects follow power-law differential size distributions with index $q = 4.0 \pm 0.5$. This slope is consistent, within the errors, with $q \approx 3.5$ as expected from a collisional production function (Dohnanyi 1969). We find no evidence in the CCD data for truncation of the size distribution at its upper end. If such truncation exists, it must occur at radii greater than 250 km. The mass of KBOs (excluding the scattered KBOs) is estimated as ~ 0.1 Earth masses.

3. About 38% (13/34 objects) of multiopposition KBOs are in the 3:2 mean motion resonance with Neptune. This "Plutino fraction" is overrepresented in the survey data as a result of observational selection. Using a bias model, we estimate that only 10%–20% of KBOs in the $R < 50$ AU region are Plutinos. If the Kuiper Belt extends beyond 50 AU, then the Plutino fraction will be considerably smaller.

4. The hypothesis that the 2:1 resonance is as densely populated as the 3:2 resonance can be rejected at the ~ 2.5 σ (98.2%) but not the 3 σ (99.7%) level of confidence. The ratio of resonance populations and the ratio of resonant to nonresonant populations are both broadly consistent with numerical simulations of the resonance-sweeping hypothesis (Malhotra 1995).

5. The observed radial distribution of KBOs is deficient in objects beyond about 50 AU, relative to simulations of power-law Kuiper Belt disks. We have no firm explanation of this observation. The Kuiper Belt might be truncated at about this distance, there might be a steep decrease in the maximum size of KBOs at larger heliocentric distances, or some combination of these two effects might conspire to yield the observed radial distribution.

size distribution cutoff at the high end). However, the Kowal (1989) datum instead falls below the extrapolated luminosity function by almost an order of magnitude. Taken at face value, the Kowal datum would require a truncation of the power-law size distribution at an upper radius limit near $r_{max} \approx 50$ km, which is problematic considering the existence of larger KBOs such as Pluto and Charon. However, we are not convinced that the photographic constraints should be taken so literally. In view of the difficulty of calibrating the efficiency of photographic surveys, we feel that it would be valuable to establish the surface density of the brightest trans-Neptunian objects using modern technology. Several thousands of square degrees should be imaged to $m_R \approx 20$. The Spacewatch camera (Scotti 1994) could usefully contribute to this search, as could the upcoming Sloan Digital Sky Survey.

4. SUMMARY

We present the results of a new ecliptic survey of 51.5 deg^2 to red limiting magnitude 22.5 (50% detection threshold).

REFERENCES

Albrecht, R., et al. 1994, ApJ, 435, L75
Altenhoff, W. J., & Stumpff, P. 1995, A&A, 293, L41
Bailey, M. E. 1994, in IAU Symp. 160, Asteroids, Comets, Meteors 1993, ed. A. Milani, M. di Martino, & A. Cellino (Dordrecht: Kluwer), 443
Bowell, E. Hapke, B., Domingue, D., Lumme, K., Peltoniemi, J., & Harris, A. W. 1989, in Asteroids II, ed. R. P. Binzel, T. Gehrels, & M. S. Matthews (Tucson: Univ. Arizona Press), 524
Brown, M. E., Kulkarni, S. R., & Liggett, T. J. 1997, ApJ, 490, L119
Campins, H., Telesco, C. M., Osip, D. J., Rieke, G. H., Rieke, M. J., & Schulz, B. 1994, AJ, 108, 2318
Cochran, A. L., Levison, H. P., Stern, S. A., & Duncan, M. J. 1995, ApJ, 455, 342
Davis, J., Spencer, J., Sykes, M., Tholen, D., & Green, S. 1993, IAU Circ. 5698
Dohnanyi, J. 1969, J. Geophys. Res., 74, 2531
Dones, L. 1997, in ASP Conf. Ser. 122, From Stardust to Planetesimals, ed. Y. J. Pendleton & A. G. G. M. Tielens (San Francisco: ASP), 347
Duncan, M. J., & Levison, H. F. 1997, Science, 276, 1670
Duncan, M. J. Levison, H. F., & Budd, S. M. 1995, AJ, 110, 3073
Duncan, M., Quinn, T., & Tremaine, S. 1988, ApJ, 328, L69
Farinella, P., & Davis, D. R. 1996, Science, 273, 938
Gladman, B., & Kavelaars, J. J. 1997, A&A, 317, 35

Holman, M. J., & Wisdom, J. 1993, AJ, 105, 1987
Ip, W.-H., & Fernandez, J. A. 1991, Icarus, 92, 185
Irwin, M., Tremain, S., & Žytkow, A. N. 1995, AJ, 110, 3082
Jewitt, D. 1996, Earth Moon Planets, 72, 185
Jewitt, D., & Luu, J. 1993, Nature, 362, 730
———. 1995, AJ, 109, 1867
———. 1998, AJ, 115, 1667
Jewitt, D., Luu, J., & Chen, J. 1996, AJ, 112, 1225
Kenyon, S., & Luu, J. 1998, AJ, submitted
Kowal, C. T. 1989, Icarus, 77, 118
Landolt, A. U. 1992, AJ, 104, 340
Levison, H. F., & Duncan, M. J. 1990, AJ, 100, 1669
Levison, H. F., & Stern, S. A. 1995, Icarus, 116, 315
Luppino, G., Metzger, M., Kaiser, N., Clowe, D., Gioia, I., & Mayazaki, S. 1996, ASP Conf. Ser. 88, Clusters, Lensing, and the Future of the Universe, ed. V. Trimble & A. Reisenegger (San Francisco: ASP), 229
Luu, J. X., & Jewitt, D. 1988, AJ, 95, 1256
———. 1996, AJ, 112, 2310
Luu, J., Marsden, B. G., Jewitt, D., Trujillo, C. A. Hergenrother, C. W., Chen, J., & Offutt, W. B. 1997, Nature, 387, 573
Malhotra, R. 1995, AJ, 110, 420
———. 1996, AJ, 111, 504

Morbidelli, A., Thomas, F., & Moons, M. 1995, Icarus, 118, 322
Morbidelli, A., & Valsecchi, G. B. 1997, Icarus, 128, 464
Scotti, J. V. 1994, in IAU Symp. 160, Asteroids, Comets, Meteors 1993, ed. A. Milani, M. di Martino, & A. Cellino (Dordrecht: Kluwer), 17
Standish, E. M., Newhall, X. X., Williams, J. G., & Folkner, W. F. 1995, JPL Planetary and Lunar Ephemerides, DE403/LE403 (Interoffice Memo. 314.10-127) (Pasadena: JPL)
Stern, S. A., & Colwell, J. E. 1997, AJ, 114, 841

Tombaugh, C. W. 1961, in Planets and Satellites, ed. G. P. Kuiper & B. M. Middlehurst (Chicago: Univ. Chicago Press), 12
Torbett, M. V. 1989, AJ, 98, 1477
Trujillo, C. & Jewitt, D. 1998, AJ, 115, 1680
Williams, I. P., O'Ceallaigh, D. P., Fitzsimmons, A., & Marsden, B. G. 1995, Icarus, 116, 180
Yamamoto, T., & Kozasa, T. 1988, Icarus, 75, 540